Supplementary Material

for

Scalable, rapid, and predictable ultraviolet-visible-near-infrared camouflage systems inspired by squid skin

Panyiming Liu,[a] Chengyi Xu,[a] Alon A. Gorodetsky[a,b*]

[a]Department of Materials Science and Engineering, University of California, Irvine, Irvine, CA 92697, USA

[b]Department of Chemical and Biomolecular Engineering, University of California, Irvine, Irvine, CA 92697, USA

[*]Correspondence to alon.gorodetsky@uci.edu

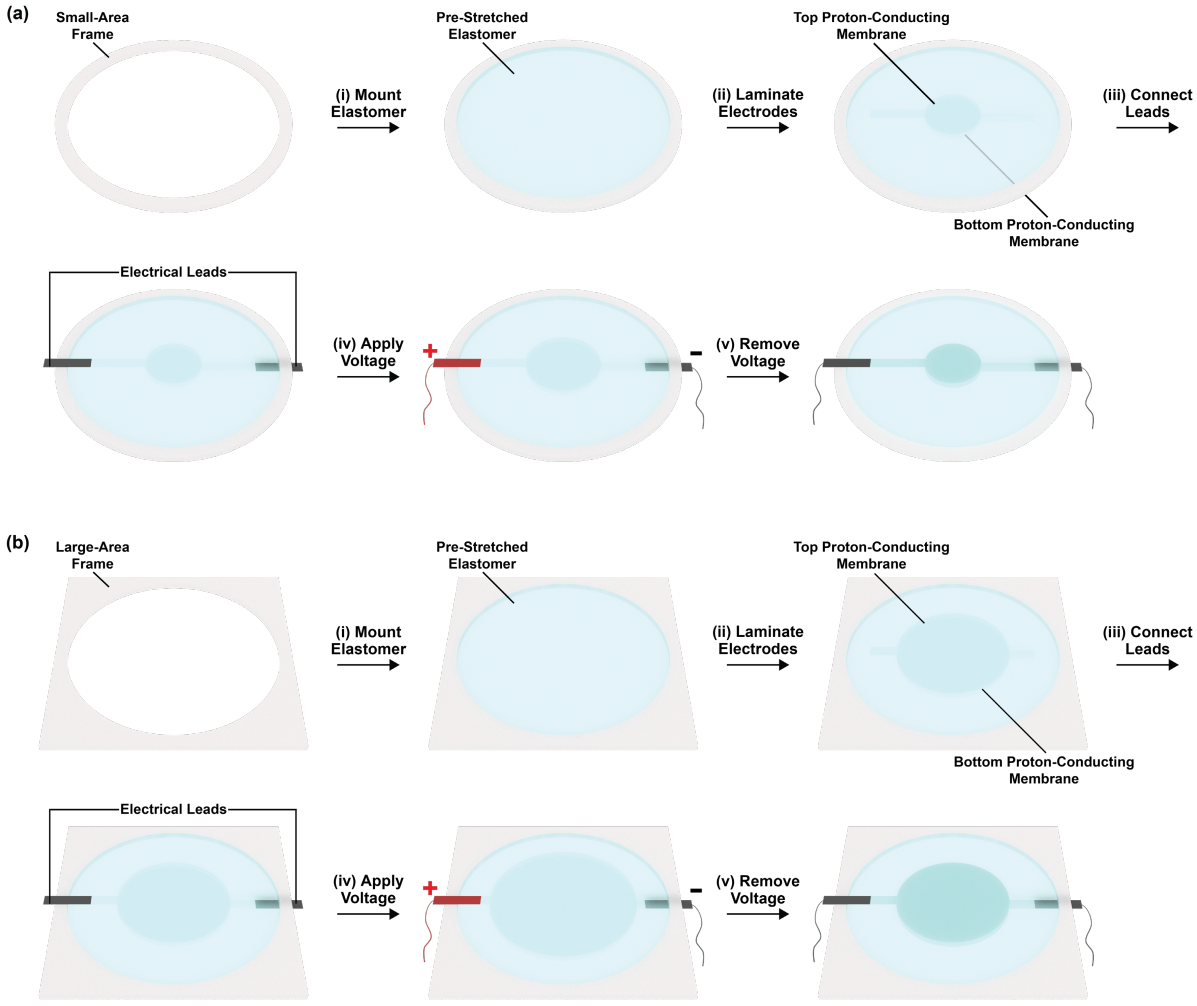

Fig. S1. Schematics illustrating the general procedure for the fabrication of **(a)** small-area devices and **(b)** large-area devices, which includes (i) mounting of transparent acrylate-based elastomer layers onto a frame, (ii) lamination of two identical proton-conducting membrane electrodes onto the elastomer layers, (iii) connection of conductive aluminum foil-based electrical leads to the laminated electrodes, (iv) the application of a voltage between the laminated electrodes to pre-condition the devices, and (v) the removal of the applied voltage to wrinkle the active regions.

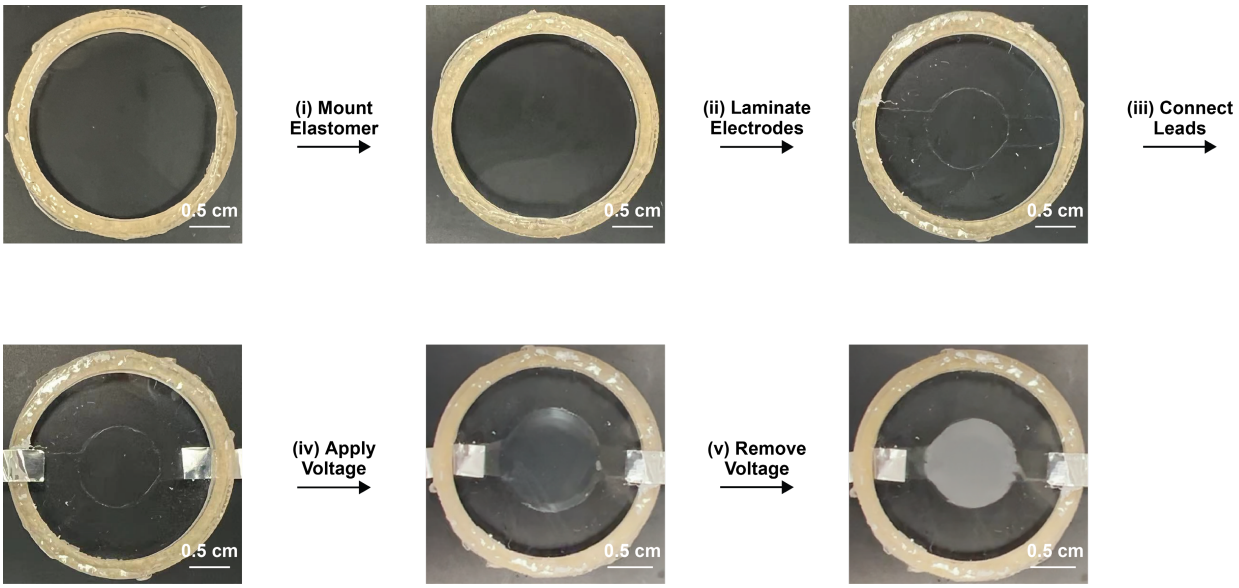

Fig. S2. Representative digital camera images obtained during the fabrication of small-area devices. The steps correspond to those shown in **Fig. S1a**.

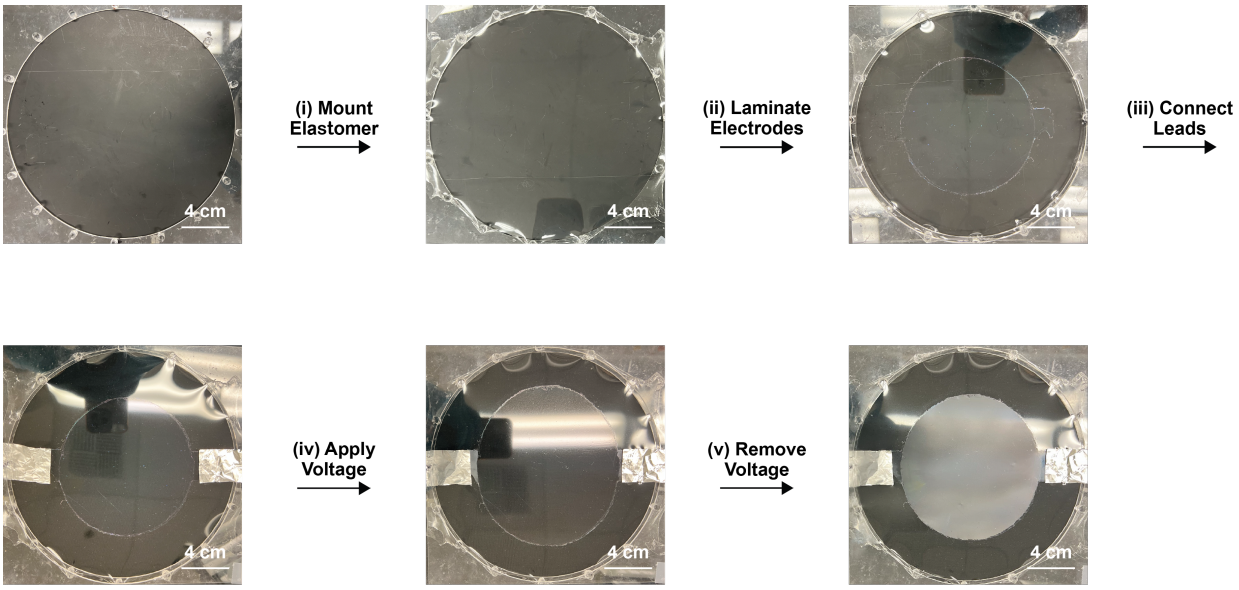

Fig. S3. Representative digital camera images obtained during the fabrication of large-area devices. The steps correspond to those shown in **Fig. S1b**.

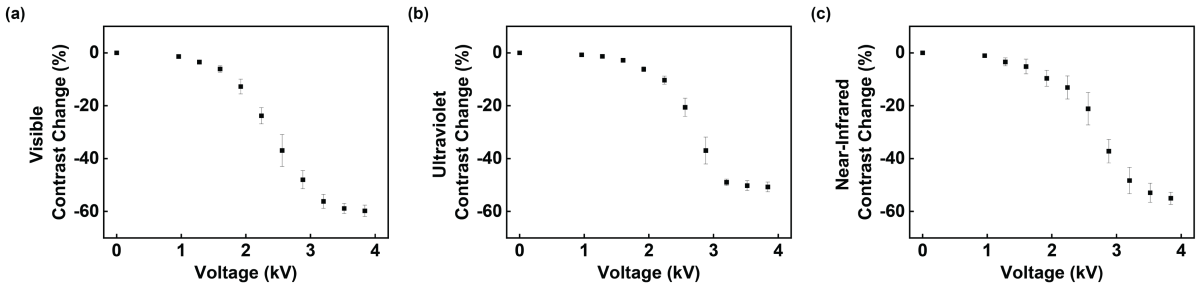

Fig. S4. (a) A plot of the visible contrast change as a function of the applied voltage for the small-area devices. **(b)** A plot of the ultraviolet contrast change as a function of the applied voltage for the small-area devices. **(c)** A plot of the near-infrared contrast change as a function of the applied voltage for the small-area devices. The devices were actuated with square waveforms (minima at 0 kV and different maxima) at a frequency of 0.05 Hz.

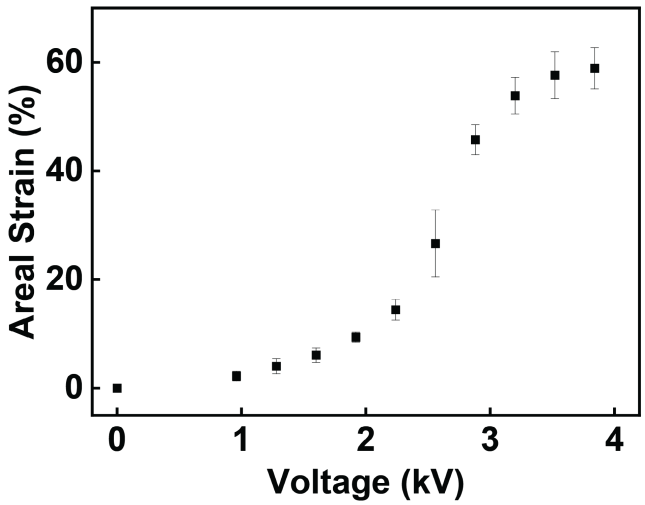

Fig. S5. A plot of the areal strain as a function of the applied voltage for the small-area devices. The devices were actuated with square waveforms (minima at 0 kV and different maxima) at a frequency of 0.05 Hz.

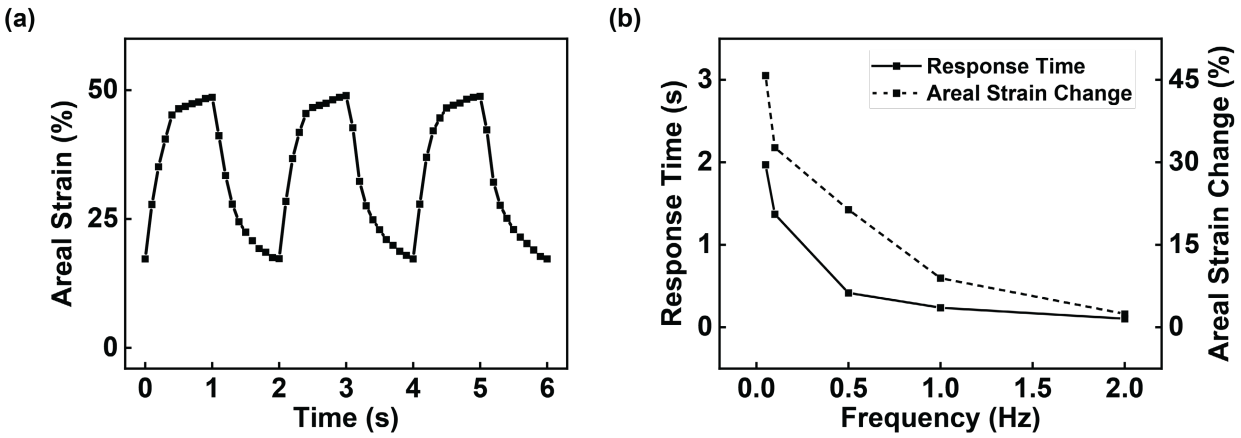

Fig. S6. (a) A representative plot of the areal strain as a function of time for a typical small-area device. **(b)** A plot of the response time and the corresponding areal strain change for the small-area devices. The devices were actuated with square waveforms (minima at 0 kV and maxima at 3.8 kV) at a frequency of 0.5 Hz in **(a)** and at variable frequencies in **(b)**.

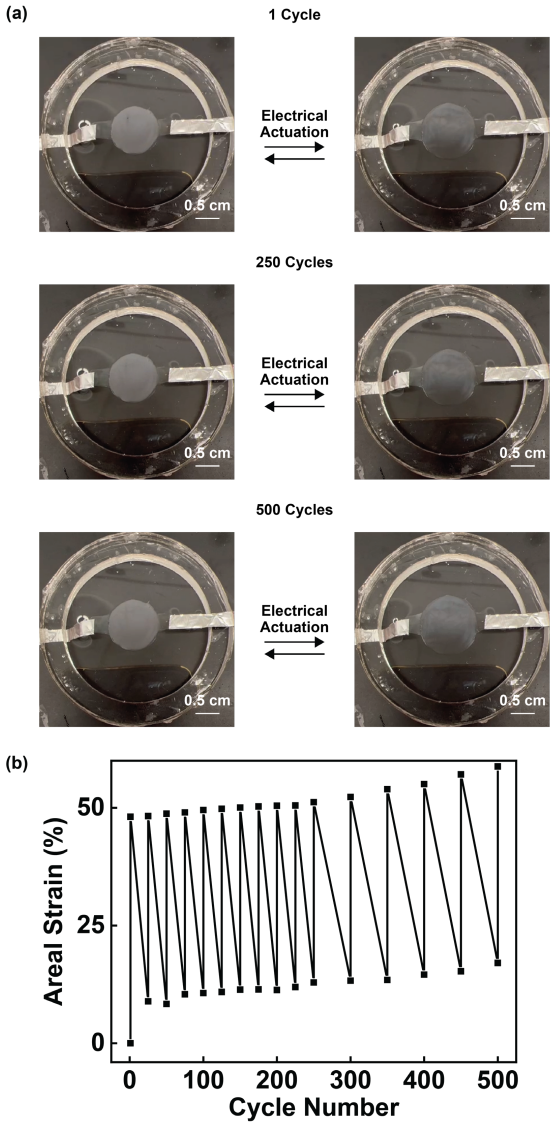

Fig. S7. (a) Representative digital camera images of a small-area device before (left) and after (right) 1, 250, and 500 electrical actuation cycles. **(b)** A representative plot of the areal strain as a function of the actuation cycle number for a typical small-area device across 500 consecutive cycles. The devices were actuated with square waveforms (minima at 0 kV and maxima at 3.8 kV) at a frequency of 0.5 Hz.

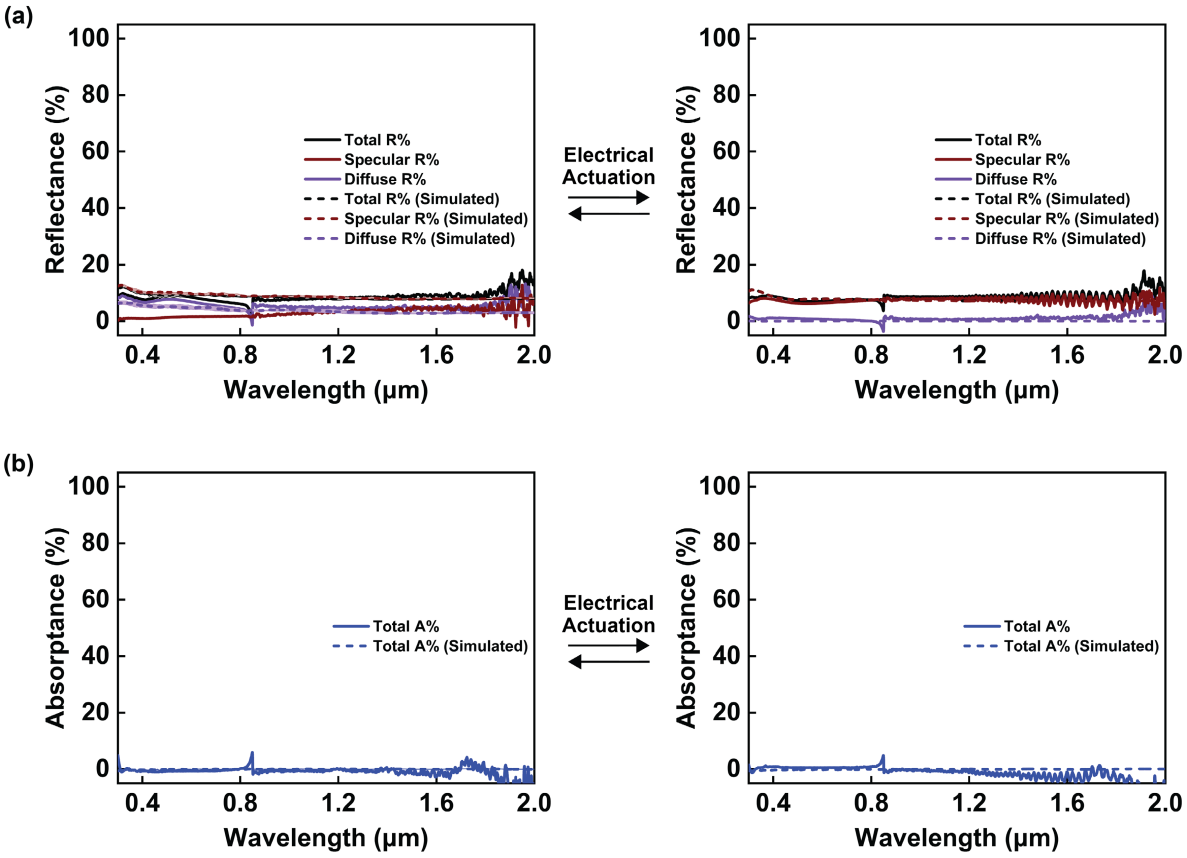

Fig. S8. (a) Representative measured total (solid black line), specular (solid brown line), and diffuse (solid purple line) reflectance spectra and representative simulated total (dashed black lined), specular (dashed brown line), and diffuse (dashed purple line) reflectance spectra for the small-area devices before (left) and (right) electrical actuation. **(b)** Representative measured absorptance spectra (solid blue line) and simulated absorptance spectra (dashed blue line) for the small-area devices before (left) and (right) electrical actuation. The devices were actuated with a 3.8 kV step voltage at a frequency of 0.05 Hz. Note that the shaded black, brown, purple, and blue regions represent multiple spectra simulated for the wrinkle geometry ranges in **Table S2**.

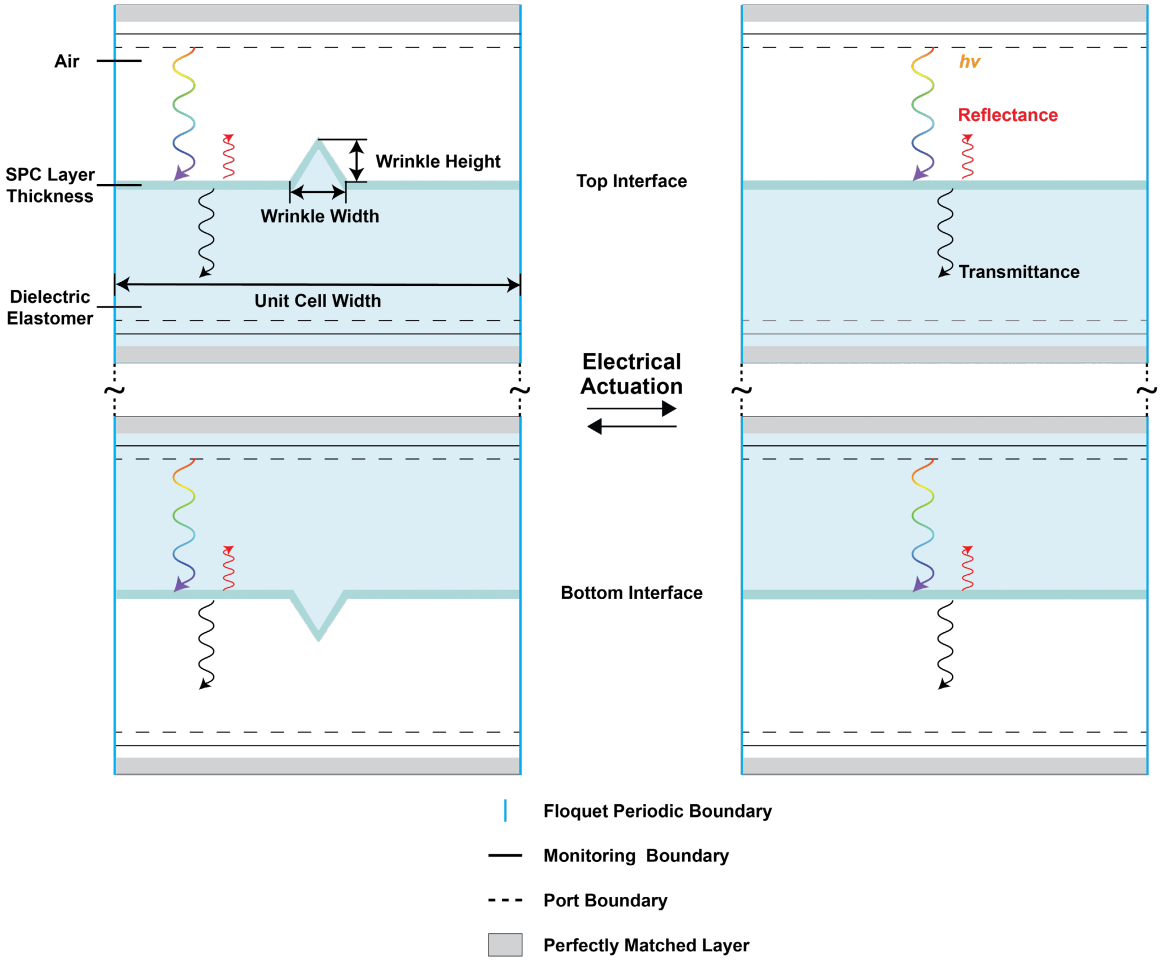

Fig. S9. Schematic of the model used to computationally simulate the ultraviolet-visible-near-infrared (UV-VIS-NIR) spectroscopic properties of the devices before (left) and after (right) electrical actuation.

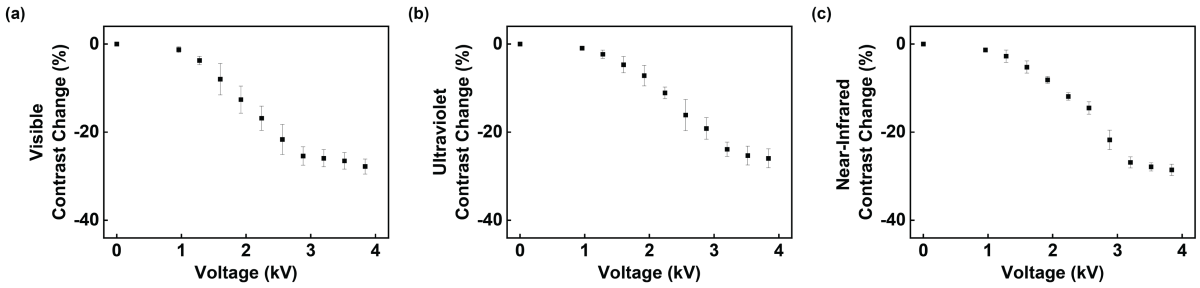

Fig. S10. (a) A plot of the visible contrast change as a function of the applied voltage for the large-area devices. **(b)** A plot of the ultraviolet contrast change as a function of the applied voltage for the large-area devices. **(c)** A plot of the near-infrared contrast change as a function of the applied voltage for the large-area devices. The devices were actuated with square waveforms (minima at 0 kV and different maxima) at a frequency of 0.05 Hz.

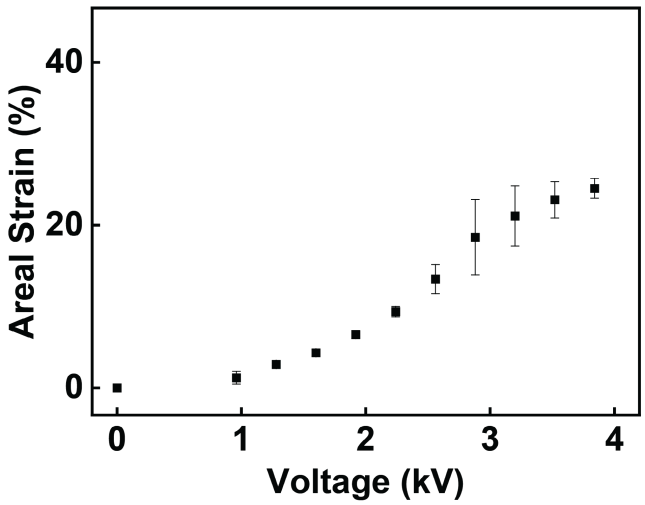

Fig. S11. A plot of the areal strain as a function of the applied voltage for the large-area devices. The devices were actuated with square waveforms (minima at 0 kV and different maxima) at a frequency of 0.05 Hz.

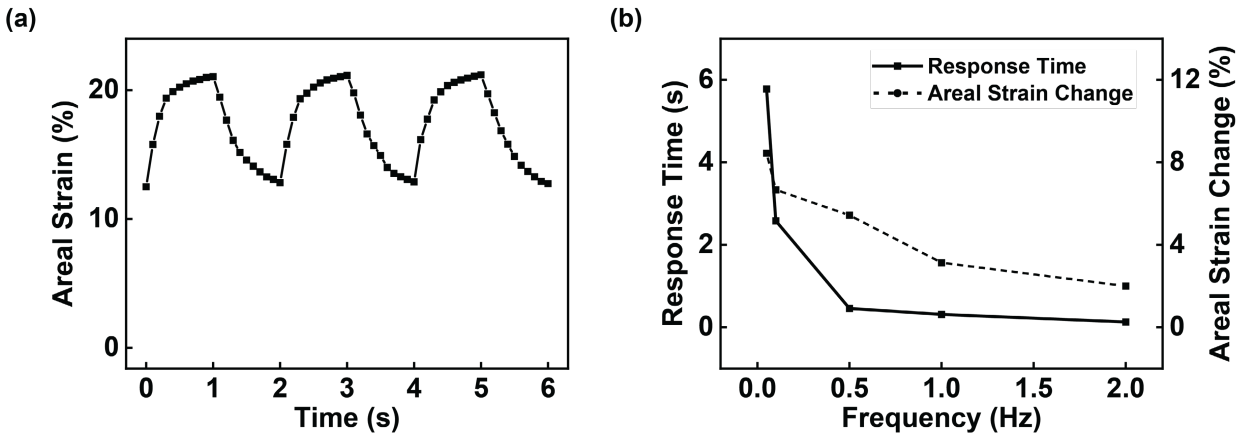

Fig. S12. (a) A representative plot of the areal strain as a function of time for a typical large-area device. **(b)** A plot of the response time and the corresponding areal strain change for the large-area devices. The devices were actuated with square waveforms (minima at 0 kV and maxima at 3.8 kV) at a frequency of 0.5 Hz in **(a)** and at variable frequencies in **(b)**.

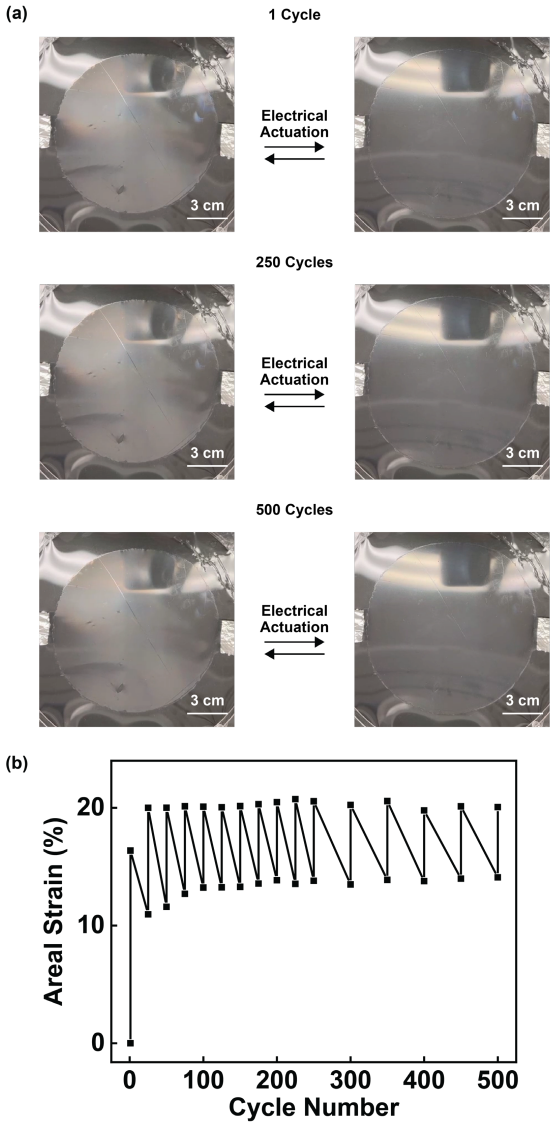

Fig. S13. (a) Representative digital camera images of a typical large-area device before (left) and after (right) 1, 250, and 500 electrical actuation cycles. **(b)** A representative plot of the areal strain as a function of the actuation cycle number for a typical large-area device across 500 consecutive cycles. The devices were actuated with square waveforms (minima at 0 kV and maxima at 3.8 kV) at a frequency of 0.5 Hz.

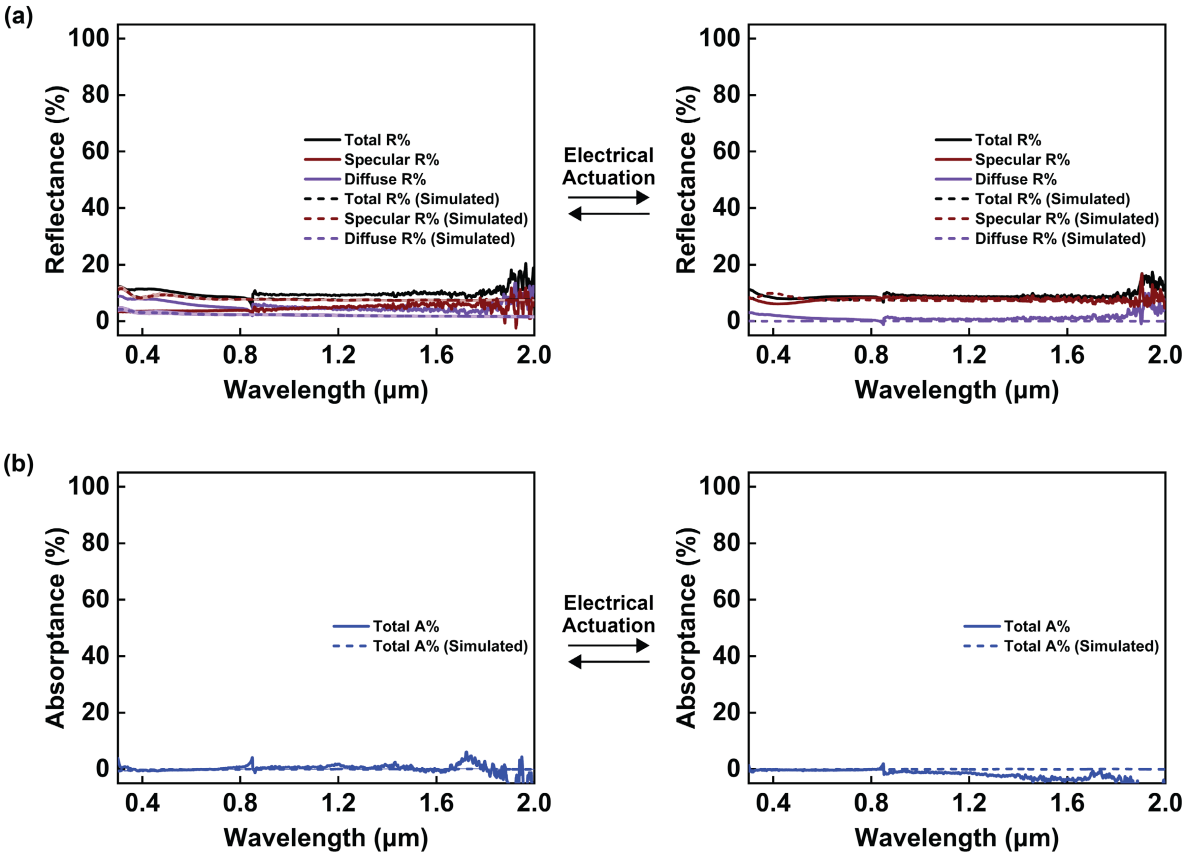

Fig. S14. (a) Representative measured total (solid black line), specular (solid brown line), and diffuse (solid purple line) reflectance spectra and representative simulated total (dashed black line), specular (dashed brown line), and diffuse (dashed purple line) reflectance spectra for the large-area devices before (left) and (right) electrical actuation. **(b)** Representative measured absorptance spectra (solid blue line) and simulated absorptance spectra (dashed blue line) for the large-area devices before (left) and (right) electrical actuation. The devices were actuated with a 3.8 kV step voltage at a frequency of 0.05 Hz. Note that the shaded black, brown, purple, and blue regions represent multiple spectra simulated for the wrinkle geometry ranges in **Table S2**.

Table S1. A summary of the key characteristics for representative surface wrinkling-based platforms reported in the literature by our laboratory and other laboratories.

Type of Platform	Actuation Approach	Spectral Range	UV, VIS, and IR Camouflage Functionality	Altered Optical Property	Specular to Diffuse Ratio Modulation	Optical Simulations	Response Time	Actuation Stability	Active Region Area	Demonstration of Scalability	Reference
Systems Developed by Our Laboratory											
Adaptive Infrared-Reflecting Systems	Electrical/ Mechanical	1.5 μm – 15.0 μm (IR)	No (only IR)	Reflectance	Reflectance: ~22-fold (IR)	Not Reported	~ 0.72 s	~ 100 Cycles	~ 0.79 cm^2	Not Reported	Xu et al., 2018[21]
Multimodal Camouflage Systems	Electrical/ Mechanical	400 nm – 16.5 μm (VIS and IR)	No (only VIS and IR)	Transmittance	Transmittance: ~ 3000-fold (VIS), ~ 4-fold (IR)	Not Reported	~ 0.57 s	~ 500 Cycles	~ 0.79 cm^2	Not Reported	Xu et al., 2020[31]
Micro- and Nano-Structured Camouflage Surfaces	Electrical/ Mechanical	400 nm – 16.0 μm (VIS and IR)	No (only VIS and IR)	Reflectance/ Transmittance/ Absorptance	Reflectance: ~ 1200-fold (VIS), ~ 5-fold (IR)	Not Reported	~ 0.70 s	~ 120 Cycles	~ 0.79 cm^2	Not Reported	Liu et al., 2021[40]
Nonacene-Based Deception and Signaling Devices	Electrical/ Mechanical	300 nm – 1.6 μm (UV, VIS, and NIR)	Yes	Absorptance/ Transmittance/ Fluorescence	Not Reported	Not Reported	~ 0.38 s	~ 500 Cycles	~ 0.95 cm^2	Not Reported	Pratakshya et al., 2023[41]
UV-VIS-NIR Camouflage Systems	Electrical/ Mechanical	300 nm – 2.0 μm (UV, VIS, and NIR)	Yes	Transmittance	Transmittance: ~ 18-fold to ~ 31-fold (UV-VIS-NIR)	Yes	~ 0.10 s	~ 500 Cycles	~ 113 cm^2	Yes	This work
Systems Developed by Other Laboratories											
Infrared Stealth Structures	Mechanical	2.0 μm – 14.0 μm (IR)	No (only IR)	Reflectance	Reflectance: ~ 28-fold (IR)	Not Reported	Not Reported	~ 500 Cycles	~ 0.16 cm^2	Not Reported	Wang et al., 2018[53]
Heat-Managing Selective Emitters	Mechanical	300 nm – 2.5 μm (VIS and NIR)	Not Applicable	Emissivity	Not Reported	Yes	Not Reported	~ 20 Cycles	~ 6.25 cm^2	Not Reported	Sala-Casanovas et al., 2019[54]
Light-to-Heat Conversion Coatings	Mechanical	300 nm – 2.5 μm (VIS and NIR)	Not Applicable	Absorptance	Not Reported	Yes	> 20 s	~ 100 Cycles	~ 60 cm^2	Yes	Li et al., 2019[55]
Rewritable Smart Optics	Mechanical and Humidity/ Temperature	300 nm – 1.0 μm (UV and VIS)	No (only UV and VIS)	Transmittance	Not Reported	Not Reported	~ 0.7 to ~ 2.8 s	~ 1000 Cycles	~ 25 cm^2	Not Reported	Jiang et al., 2019[56]
Thermochromic Strain Sensors	Mechanical	400 nm – 700 nm (VIS)	Not Applicable	Reflectance	Not Reported	Not Reported	~ 0.5 s	~ 1000 Cycles	~ 48 cm^2	Not Reported	Lee et al., 2020[57]
Tunable Optical Cavities	Mechanical/ Temperature	400 nm – 1.2 μm (VIS and NIR)	Not Applicable	Reflectance	Not Reported	Yes	Not Reported	Not Reported	~ 1 cm^2	Not Reported	Güell-Grau et al., 2021[58]
Photothermal Electromagnetic Shielding	Mechanical	Range Not Specified (IR)	Not Applicable	Absorptance/ Transmittance	Not Reported	Yes	~ 60 s	~ 200 Cycles	~ 50 cm^2	Not Reported	Yu et al., 2024[59]

Table S2. The tabulated geometric and optical input parameters used to simulate the UV-VIS-NIR spectroscopic properties of the small-area and large-area devices.

Parameter name	Symbol	Unit	Value for Small-Area Devices		Value for Large-Area Devices	
			Before Actuation	After Actuation	Before Actuation	After Actuation
Wrinkle Height	$H_{wrinkle}$	[μm]	0.475 ± 0.038[a]	0[b]	0.343 ± 0.049[a]	0[b]
Wrinkle Width	$W_{wrinkle}$	[μm]	1.53 ± 0.07[a]	0[b]	1.55 ± 0.16[a]	0[b]
Wrinkle Peak-to-Peak Distance	$D_{wrinkle}$	[μm]	10.1 ± 0.7[a]	10.1[c]	14.9 ± 1.6[a]	14.9[c]
SPC Layer Thickness	Th_{SPC}	[μm]	0.25[d]			
SPC Refractive Index	$\bar{n}_{SPC}$	—	1.510 at 589 nm[e]			
Dielectric Elastomer Refractive Index	$\bar{n}_{acrylate}$	—	1.492 at 589 nm[f]			
Air Refractive Index	$\bar{n}_{air}$	—	1[g]			

[a] The average values were estimated from measurements performed with a Cypher ES environmental AFM (Asylum), and the average values plus or minus one standard deviation were used for the simulations.
[b] The average values were assumed to be zero after actuation due to the absence of large wrinkles.
[c] The average values corresponding to the unit cell width were assumed to remain unchanged after actuation.
[d] The average values were estimated from experimental measurements performed with an F2-RT spectrometer (Filmetrics).
[e] The wavelength-dependent $\bar{n}_{SPC}$ values (300 nm to 2 μm) were estimated from experimental measurements performed with an F20-UV spectrometer (Filmetrics) and were used for the simulations.
[f] The wavelength-dependent $\bar{n}_{acrylate}$ values (300 nm to 2 μm) were obtained from the literature and were used for the simulations[68].
[g] The wavelength-dependent $\bar{n}_{air}$ values (300 nm to 2 μm) for air were obtained from the literature and were used for the simulations[69].

Table S3. The tabulated average values of the measured and simulated total reflectances, transmittances, and absorptances; specular and diffuse transmittances and reflectances; and specular-to-diffuse transmittance and specular-to-diffuse reflectance ratios for both the small-area and large-area devices before and after electrical actuation.

Device Type / Optical Property	Small-Area Devices				Large-Area Devices			
	Measured (Unactuated)	**Measured (Actuated)**	**Simulated (Unactuated)**	**Simulated (Actuated)**	**Measured (Unactuated)**	**Measured (Actuated)**	**Simulated (Unactuated)**	**Simulated (Actuated)**
Total Transmittance (%)	91 ± 2	93 ± 1	91 ± 1	93	90 ± 2	93 ± 1	92 ± 1	93
Total Reflectance (%)	9 ± 1	8 ± 1	9 ± 1	7	9 ± 1	9 ± 1	8 ± 1	7
Total Absorptance (%)	0 ± 1	0 ± 1	0 ± 1	0	1 ± 1	0 ± 1	0 ± 1	0
Specular Transmittance (%)	67 ± 2	92 ± 1	73 ± 3	92	74 ± 2	92 ± 1	83 ± 3	92
Specular Reflectance (%)	3 ± 1	7 ± 1	4 ± 1	7	4 ± 1	8 ± 1	6 ± 1	7
Diffuse Transmittance (%)	24 ± 1	1 ± 1	18 ± 3	1	16 ± 1	1 ± 1	9 ± 3	1
Diffuse Reflectance (%)	6 ± 1	1 ± 1	5 ± 1	0	5 ± 1	1 ± 1	2 ± 1	0
Specular to Diffuse Transmittance Ratio	3	92	4	92	5	92	9	92
Specular to Diffuse Reflectance Ratio	0.5	7	0.8	> 7	0.8	8	3	> 7

Video S1. Representative video of a small-area device under visible light illumination during cyclical electrical actuation with a square-waveform (minima at 0 kV and maxima at 3.8 kV) at a frequency of 0.5 Hz. Note that the video has been sped up by 4X.

Video S2. Representative video of a small-area device under ultraviolet light illumination during cyclical electrical actuation with a square-waveform (minima at 0 kV and maxima at 3.8 kV) at a frequency of 0.5 Hz. Note that the video has been sped up by 4X.

Video S3. Representative video of a small-area device under near-infrared light illumination during cyclical electrical actuation with a square-waveform (minima at 0 kV and maxima at 3.8 kV) at a frequency of 0.5 Hz. Note that the video has been sped up by 4X.

Video S4. Representative video of a large-area device under visible light illumination during cyclical electrical actuation with a square-waveform (minima at 0 kV and maxima at 3.8 kV) at a frequency of 0.5 Hz. Note that the video has been sped up by 4X.

Video S5. Representative video of a large-area device under ultraviolet light illumination during cyclical electrical actuation with a square-waveform (minima at 0 kV and maxima at 3.8 kV) at a frequency of 0.5 Hz. Note that the video has been sped up by 4X.

Video S6. Representative video of a large-area device under near-infrared light illumination during cyclical electrical actuation with a square-waveform (minima at 0 kV and maxima at 3.8 kV) at a frequency of 0.5 Hz. Note that the video has been sped up by 4X.